Journal of Alloys and Compounds xxx (2009) xxx–xxx

Contents lists available at ScienceDirect

Journal of Alloys and Compounds

journal homepage: www.elsevier.com/locate/jallcom

Physical properties of In_2O_3 thin films prepared at various oxygen partial pressures

S. Kaleemulla [a,*], A. Sivasankar Reddy [c], S. Uthanna [b], P. Sreedhara Reddy [b]

[a] Department of Physics, Vellore Institute of Technology, Vellore 632014, India
[b] Department of Physics, Sri Venkateswara University, Tirupati 517502, India
[c] Department of Mechanical Engineering, University of Coimbra, Coimbra, Portugal

ARTICLE INFO

Article history:
Received 7 September 2008
Received in revised form 1 January 2009
Accepted 6 January 2009
Available online xxx

PACS:
68.55.Jk
73.61.r
78.55.m

Keywords:
Indium oxide
Activated reactive evaporation
Transparent conducting oxide
Photoluminescence

ABSTRACT

Polycrystalline cubic In_2O_3 thin films were deposited on the normal glass substrates by activated reactive evaporation method and systematically investigated the influence of oxygen partial pressure on the structural, optical, electrical and photoluminescence properties of the films. X-ray diffraction studies revealed that the films formed at oxygen partial pressure of 2×10^{-3} mbar were nearly stoichiometric. The films formed at an oxygen partial pressure of 2×10^{-3} mbar exhibited the electrical resistivity of 8.2×10^{-4} Ω cm, optical transmittance of 87% and the optical band gap of 3.62 eV. Two distinct emission peaks in the photoluminescence spectrum were observed at 415 and 440 nm in the visible region of the solar spectrum.

1. Introduction

Non-stoichiometric transparent conducting oxides (TCO) such as tin oxide, cadmium oxide, zinc oxide, indium oxide, etc., find a wide variety of applications in microelectronic and optoelectronic devices because of their high optical transmittance in the visible range with high electrical conductivity. Among these, indium oxide (In_2O_3) is an n-type degenerate semiconducting oxide which is finds optoelectronic applications such as flat panel displays, solar cells, photodiodes [1–3], etc. For the past three decades many researchers have reported on the physical properties of In_2O_3 films formed by different deposition methods such as flash evaporation [4], electron beam evaporation [5], dc/rf magnetron sputtering [6–8], laser deposition [9], molecular beam epitaxy [10], chemical vapor deposition [11,12], sol–gel process [13], spray pyrolysis [14,15], electrochemical deposition [16] were employed for preparing indium oxide films to meet present day science and technological requirements. But less work has been reported on the influence of oxygen partial pressure (pO_2) which affects the physical properties of In_2O_3 films prepared by activated reactive evaporation method.

The objective of this study is to investigate the effect of oxygen partial pressure (pO_2) on the structural, optical, electrical and photoluminescence properties of In_2O_3 thin films prepared by high density plasma enhanced activated reactive evaporation method at lower substrate temperatures.

2. Experimental

Thin films of In_2O_3 were prepared by using a home built activated reactive evaporation (ARE) system. The schematic of the ARE setup is shown in Fig. 1. The vacuum system consisted of a diffusion pump backed by a rotory pump. The pressure in the vacuum chamber was measured using Pirani and Penning gauges. After attaining the base pressure of 3×10^{-6} mbar, pure oxygen gas (99.999%) was admitted in the vacuum chamber through a fine controlled needle value. The flow of the reactive gas of oxygen was controlled by Tylon mass flow controller (MFC). Pure indium (99.999%) was used as a source material for the deposition of the films. A DC power supply of 1000 V with 1 A was used to produce the discharge near the substrate. The In_2O_3 films were deposited on well cleaned glass substrates held at temperature of 573 K under various oxygen partial pressures in the range 5×10^{-4} to 5×10^{-3} mbar. The deposition conditions maintained during the preparation of the films are given in Table 1. The deposited films were characterized for the chemical composition, crystallographic structure, electrical, optical and photoluminescence properties. The thickness of the films was determined from the interference of the optical transmittance spectra. The chemical composition of the films was analyzed by energy dispersive X-ray analysis (EDAX) attached to the scanning electron microscope (JSM-840A). The crystallographic structure of the films was

* Corresponding author at: Department of Physics, Vellore Institute of Technology, Vellore 632014, India. Tel.: +91 988 57 94010; fax: +91 877 22 49685.
E-mail address: skaleemulla@gmail.com (S. Kaleemulla).

0925-8388/$ – see front matter © 2009 Elsevier B.V. All rights reserved.
doi:10.1016/j.jallcom.2009.01.003

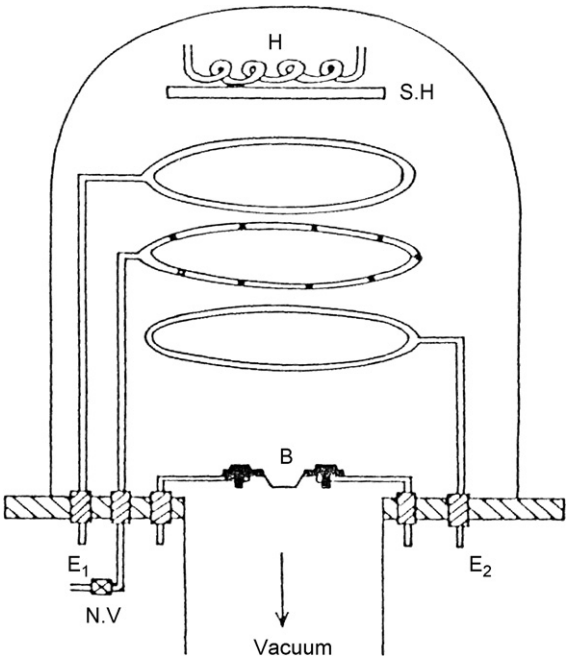

Fig. 1. Schematic representation of activated reactive evaporation technique (E_1, E_2: Electrodes; B: Boat; N.V.: Needle valve; H: Substrate heater; S.H.: Substrate holder).

determined by employing Seifert X ray diffractometer using the copper kα radiation of 1.5406 Å. The surface morphology of the films was examined by atomic force microscope (Veeco-CP-2). The optical transmittance of the films was recorded using Hitachi U-3400 UV–VIS-NIR double beam spectrophotometer in the wavelength range 300–1500 nm. The photoluminescence spectrum of the films was recorded in the wavelength range, 400–500 nm using photoluminescence spectrophotometer (Model:Yvon Fluorolog3). The electrical resistivity of the deposited films was measured using standard van der Pauw method [17]. The electrical current was applied using Advantest programmable DC voltage/current generator (Model: TR 6142) and the voltage drop across the film was measured with Hewlett Packard multimeter. Hall voltage developed in the films was measured by applying a magnetic field of 0.8 T and used for the determination of Hall mobility and carrier concentration.

The sheet resistance (ρ_s) of the films was determined using the relation

$$\rho_s = \left(\frac{\pi}{\ln 2}\right) f \left[\frac{(R_1 + R_2)}{2}\right] \quad (1)$$

where f is the van der Pauw correction factor, which depends on the position of electrical contacts on the film surface and can be obtain from the relation

$$f = \left(\frac{1 - \ln 2}{2}\right) \left[\frac{(R_1 - R_2)}{(R_1 + R_2)}\right]^2 \quad (2)$$

The electrical resistivity (ρ) of the films was determined from the relation

$$\rho = \rho_s t \quad (3)$$

where t is the thickness of the film. The Hall Mobility (μ) of the films was evaluated from the relation

$$\mu = \frac{(\Delta R \times 10^8)}{B\rho_s} \quad (4)$$

where ΔR is the change in the electrical resistance with the applied magnetic field of B.

Table 1
Deposition parameters during the preparation of In_2O_3 films.

Source material	: Indium (99.999%)
Substrates	: Corning 7059 glass
Source to substrate distance	: 100 mm
Base pressure in the chamber	: 3×10^{-6} mbar
Oxygen partial pressure (pO_2)	: 5×10^{-4} to 5×10^{-3} mbar
Substrate temperature (T_s)	: 573 K

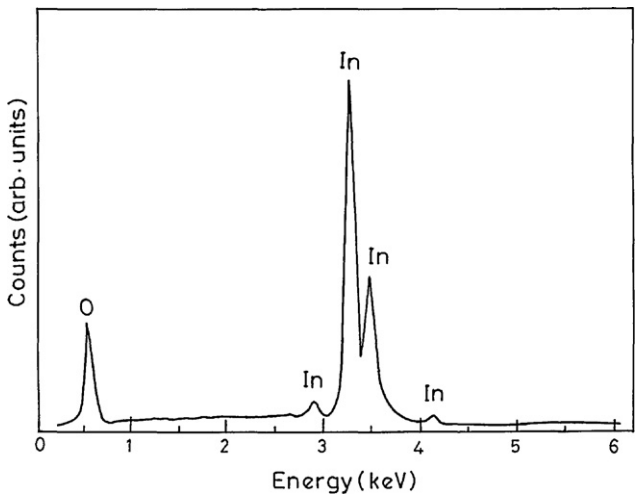

Fig. 2. EDAX spectrum of the In_2O_3 films formed at a pO_2 of 2×10^{-3} mbar.

3. Results and discussion

3.1. Structural properties of In_2O_3 thin films

The chemical composition analysis was carried out using energy dispersive analysis of X-rays. A representative EDAX spectrum of the film formed at an oxygen partial pressure of 2×10^{-3} mbar is shown in Fig. 2. The atomic concentration of the films formed at different oxygen partial pressures are given in Table 2. The films deposited at lower oxygen partial pressure of 5×10^{-4} mbar showed atomic ratio of O to In of 0.86 which indicated the indium rich in the films. The atomic ratio of O to In of the films deposited at an oxygen partial pressure of 2×10^{-3} mbar was 1.02 which indicated that the films were nearly stoichiometric In_2O_3. When the oxygen partial pressure further increased to 5×10^{-3} mbar, the atomic ratio of O to In of the films decreased to 0.97 due to excess of oxygen. The EDAX analysis revealed that the nearly stoichiometric films were obtained at an oxygen partial pressure of 2×10^{-3} mbar.

Fig. 3 shows the X-ray diffraction patterns of the films formed at different oxygen partial pressures. The diffraction peaks indicated that the films were polycrystalline with cubic structure. The films formed at lower oxygen partial pressure exhibited indium peak indicated the deficiency of oxygen. As the oxygen partial pressure increased, single phase polycrystalline films were observed with predominant (2 2 2) orientation. The intensity of the diffracted (2 2 2) peak increased with the increase of oxygen partial pressure while the Indium peak of (1 0 1) was disappeared at $pO_2 \geq 2 \times 10^{-3}$ mbar. It suggested that the crystallinity of the In_2O_3 films increased with the increase of oxygen partial pressure. This is similar to the result observed in DC magnetron sputtered CdO films formed at lower oxygen partial pressure [18].

The mean crystallite size (L) of the In_2O_3 films was calculated by using Scherrer's relation [19],

$$L = \frac{k\lambda}{\beta \cos\theta} \quad (5)$$

Table 2
Chemical composition of the In_2O_3 films formed at various oxygen partial pressures.

pO_2 (mbar)	Atomic percentages		
	Oxygen	Indium	Oxygen/Indium
5×10^{-4}	46.4	53.6	0.86
1×10^{-3}	47.2	52.8	0.89
2×10^{-3}	49.5	50.5	1.02
5×10^{-3}	52.8	51.2	0.97

Please cite this article in press as: S. Kaleemulla, et al., J. Alloys Compd. (2009), doi:10.1016/j.jallcom.2009.01.003

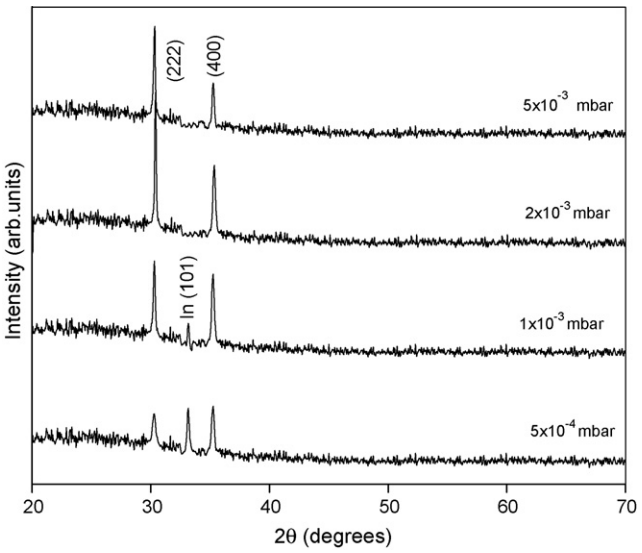

Fig. 3. X-ray diffraction patterns of the In_2O_3 films prepared at various oxygen partial pressures.

where k is a constant, λ the wavelength of the X-rays, β the full width at half maximum (FWHM) and θ the Bragg's diffraction angle. The crystallite size of the In_2O_3 films varied from 11 to 25 nm with the increase of oxygen partial pressure in the range 5×10^{-4} to 2×10^{-3} mbar, respectively thereafter it slightly decreased to 21 nm at higher oxygen partial pressure of 5×10^{-3} mbar. The lattice parameter of the films determined from the (2 2 2) reflection was increased from 10.108 to 10.115 Å with the increase of oxygen partial pressure from 5×10^{-4} to 5×10^{-3} mbar. The lattice parameters obtained are lower than the bulk material value of 10.118 Å [20]. This may be due the phenomenon of lattice contraction developed in the films. But no significant effect of oxygen partial pressure on the lattice constant was observed in vacuum evaporated In_2O_3 films [21].

Fig. 4 shows the surface morphology of the film formed at an oxygen partial pressure of 2×10^{-3} mbar obtained by scanning electron microscope. From this it was found that the films showed large number of small uniform spherical grains over the entire surface with average grain size of 26 nm. Fig. 5 represents the surface topography of the films formed at an optimum oxygen partial pressure of

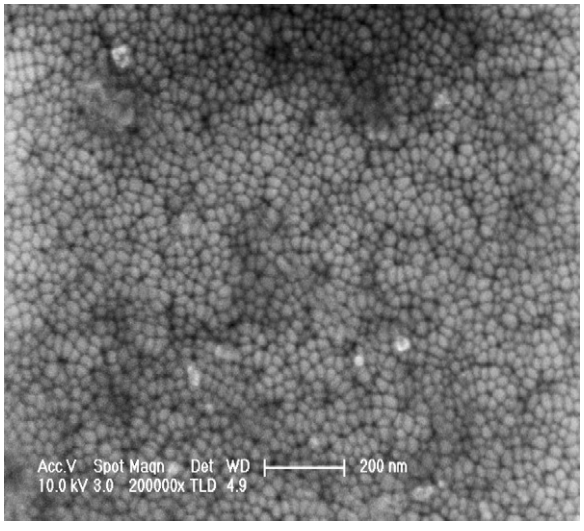

Fig. 4. Scanning electron microscope image of the In_2O_3 film formed at a pO_2 of 2×10^{-3} mbar.

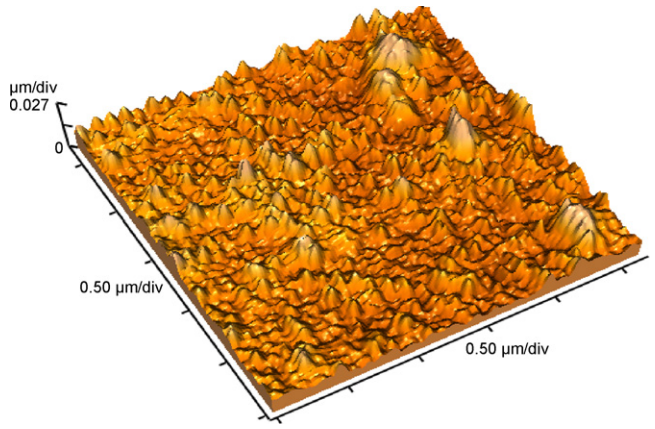

Fig. 5. Atomic force microscope image of the In_2O_3 film formed at a pO_2 of 2×10^{-3} mbar.

2×10^{-3} mbar achieved by atomic force microscope. The films were having homogeneous, smooth surface with pyramid shape grains. The average roughness of the films was found to be as 1.7 nm.

3.2. Optical properties of In_2O_3 films

Fig. 6 shows the optical transmittance spectra of the In_2O_3 films formed at various oxygen partial pressures. The films formed at lower oxygen partial pressure of 5×10^{-3} mbar exhibited low optical transmittance (T) of about 72%. The low optical transmittance at lower oxygen partial pressure may be due to insufficient oxygen available for reaction of indium with oxygen to form indium oxide. It is also conformed in X-ray diffraction patterns in which un-oxidized indium peak was observed at lower oxygen partial pressures. The un-oxidized indium acts as scattering centers for light hence of low optical transmittance at lower oxygen partial pressures. The films with light yellow color were observed at lower oxygen partial pressure after which they converted to colorless at oxygen partial pressures $\geq 2 \times 10^{-3}$ mbar which is the characteristic of increase in the optical transmittance of the films. The increase of optical transmittance at oxygen partial pressures $\geq 2 \times 10^{-3}$ mbar was due to the decrease of scattering centers of light because of formation of nearly stoichiometric hence improved the optical transmittance.

Fig. 7 shows the variation of absorption coefficient (α) of the In_2O_3 films with the oxygen partial pressure. From the figure it observed that the absorption coefficient decreased with the

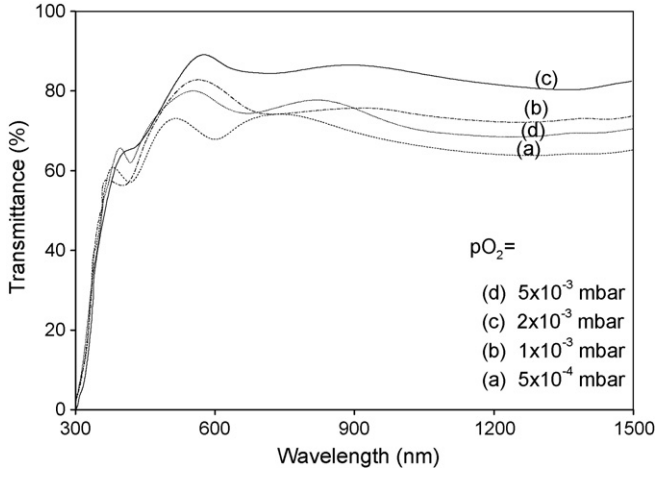

Fig. 6. Optical transmittance spectra of the In_2O_3 films formed at various oxygen partial pressures.

Please cite this article in press as: S. Kaleemulla, et al., J. Alloys Compd. (2009), doi:10.1016/j.jallcom.2009.01.003

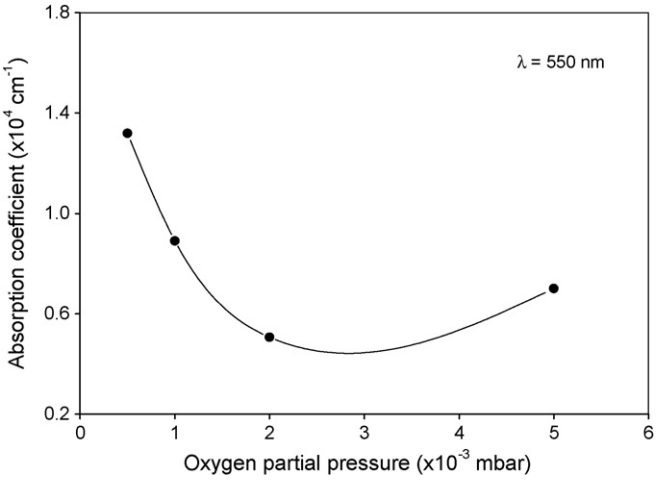

Fig. 7. Variation of the absorption coefficient of the In_2O_3 films with the oxygen partial pressure.

increase of oxygen partial pressure. The films exhibited a higher absorption coefficient of $1.3 \times 10^4\ cm^{-1}$ at a lower oxygen partial pressure of 5×10^{-4} mbar. Then it decreased to $0.5 \times 10^4\ cm^{-1}$ at a higher oxygen partial pressure of 2×10^{-3} mbar.

The optical band gap (E_g) of the films was determined from the optical transmittance data using Tauc's relation [22],

$$(\alpha h\nu) = (E_g - h\nu)^n \quad (6)$$

where n depend on the kind of optical transition that prevails. Here $n = 1/2$, as In_2O_3 films are directly allowed n-type degenerate semiconductors. The optical bang gap is obtained by plotting $(\alpha h\nu)^2$ versus the photon energy ($h\nu$) and by extrapolating of the linear region of the plots to zero absorption ($\alpha = 0$). It increased from 3.59 to 3.64 eV with the increase of oxygen partial pressure in the range 5×10^{-4} to 5×10^{-3} mbar.

3.3. Electrical properties of In_2O_3 films

Fig. 8 shows the variation of electrical resistivity and carrier concentration of the In_2O_3 films formed at various oxygen partial pressures in the range 5×10^{-4} to 5×10^{-3} mbar. The films formed at lower oxygen partial pressure of 5×10^{-4} mbar exhibited a minimum resistivity of $8.2 \times 10^{-4}\ \Omega$ cm. In general, the electrical resistivity of the transparent conducting oxide can be decreased by increasing oxygen vacancies or by adding suitable dopants to the parent matrix [23]. As the oxygen partial pressure increased to 5×10^{-3} mbar, the electrical resistivity of the films also increased to $1.8 \times 10^{-3}\ \Omega$ cm. The low electrical resistivity at lower oxygen partial pressures was due to presence of additional phase of indium as observed in the X-ray diffraction patterns. At oxygen partial pressures $\geq 2 \times 10^{-3}$ mbar indium phase disappeared, leading to the formation of stoichiometric In_2O_3 films, hence the increase in the electrical resistivity of the In_2O_3 films. Hall mobility measurement indicated that the films were n-type. Hall mobility of the films increased from 18 to 25.5 $cm^2/V\,s$ with the increase of oxygen partial pressure from 5×10^{-4} to 2×10^{-3} mbar, thereafter it decreased to 21 $cm^2/V\,s$ at higher oxygen partial pressure of 5×10^{-3} mbar. Such a variation in the electrical resistivity was also observed in DC reactive magnetron sputtered cadmium oxide films [24]. The carrier concentration of the films decreased from 4.2×10^{20} to $2.5 \times 10^{20}\ cm^{-3}$ with the increase of oxygen partial pressure from 5×10^{-4} to 2×10^{-3} mbar. The high carrier concentration at lower oxygen partial pressure was due to the presence of un-oxidized indium in the films while at oxygen partial pressures $\geq 2 \times 10^{-3}$ mbar, the films were nearly stoichiometric hence the decrease in the carrier concentration.

Table 3
Sheet resistance, optical transmittance and figure of merit of the In_2O_3 films.

pO_2 (mbar)	Sheet resistance ($\Omega/\square$)	Optical transmittance (%)	Figure of merit ($\times 10^{-3}\ \Omega^{-1}$)
5×10^{-4}	32.0	72	1.14
1×10^{-3}	36.4	80	2.94
2×10^{-3}	38.8	87	6.40
5×10^{-3}	72.0	82	1.90

The performance of the TCO material can be determined from the sheet resistance (ρ_s) and optical transmittance using Haacke's the figure of merit (Φ) relation [25],

$$\Phi_{TC} = \frac{T^{10}}{\rho_s} \quad (7)$$

where T is the transmittance at 550 nm. The summary of sheet resistance, optical transmittance and figure of merit of the films are shown in Table 3.

Fig. 9 shows the variation of the figure of merit at different oxygen partial pressures. Generally, a film with low electrical resistivity and high optical transmittance would have a relatively high fig-

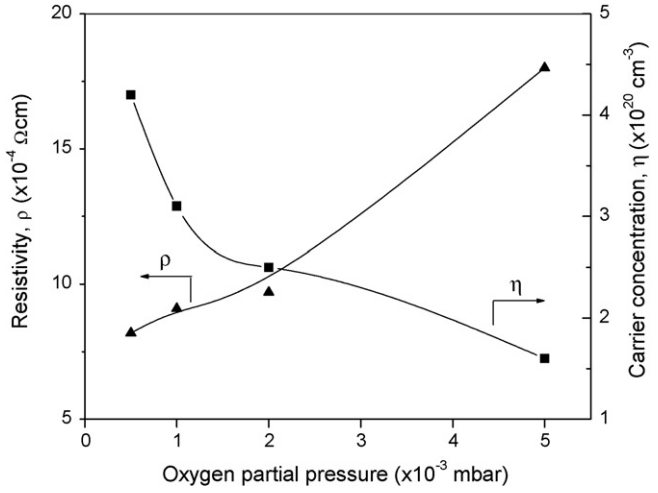

Fig. 8. Variation of electrical resistivity (ρ) and carrier concentration (n) of the In_2O_3 films with the oxygen partial pressure.

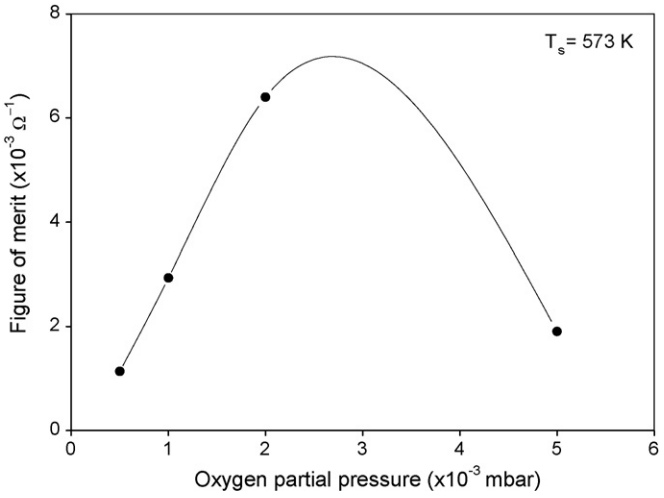

Fig. 9. Variation in the figure of merit of the In_2O_3 films with the oxygen partial pressure.

Please cite this article in press as: S. Kaleemulla, et al., J. Alloys Compd. (2009), doi:10.1016/j.jallcom.2009.01.003

Table 4
Comparison of the figure of merit of undoped and doped In_2O_3 films formed by different deposition methods.

Material	Deposition technique	pO_2 (mbar)	T_s (K)	Φ ($\times 10^{-3}\ \Omega^{-1}$)	Reference
In_2O_3	DC magnetron sputtering	2.0×10^{-4}	673	1.2	[6]
In_2O_3	Activated reactive evaporation	2.0×10^{-3}	573	6.4	Present work
In_2O_3:Sn	Activated reactive evaporation	1.8×10^{-4}	623	21	[26]
In_2O_3:Sn	Reactive evaporation	1.0×10^{-4}	403	0.4	[27]
In_2O_3:Mo	DC magnetron sputtering	3.8×10^{-4}	313	7.5	[28]
In_2O_3:Mo	High density plasma evaporation	–	303	12.6	[29]

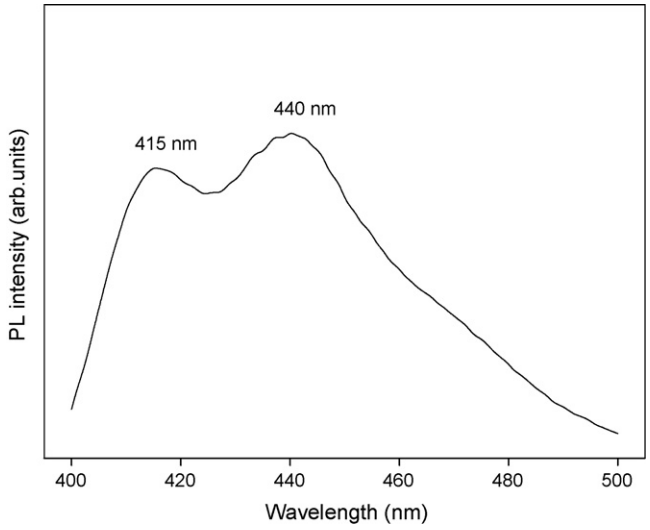

Fig. 10. Photoluminescence (PL) spectrum of the In_2O_3 film formed at a pO_2 of 2×10^{-3} mbar.

ure of merit. The films formed at lower oxygen partial pressure of 5×10^{-4} mbar, exhibited the figure of merit of $1.14 \times 10^{-3}\ \Omega^{-1}$ and then it increased to $6.4 \times 10^{-3}\ \Omega^{-1}$ at higher oxygen partial pressure of 2×10^{-3} mbar. Table 4 shows the comparison of the figure of merit of undoped and doped In_2O_3 thin films formed by different deposition methods.

3.4. Photoluminescence property of In_2O_3 films

Fig. 10 shows the emission photoluminescence (PL) spectrum of indium oxide thin films formed on glass substrates. Two distinct peaks in the PL spectrum were observed in the blue region, i.e. at wavelengths of 415 and 440 nm wavelength under the excitation wavelength of 375 nm at room temperature. Lee et al. [30] had observed the photoluminescence at room temperature in orange region in the In_2O_3 films deposited on Si and Mo substrates. In the literature, strong peaks were observed at 470 and 1540 nm in single crystalline In_2O_3 films [31] and erbium doped In_2O_3 films [32], respectively. However further investigation is required for the exact origin of photoluminescence and energy levels responsible for the observed emission peaks. One of the possible reasons is explained as follows. When the indium oxide films were prepared at high temperature, oxygen vacancies and oxygen-indium vacancy pairs might have been produced. Therefore, it is believed that the intense blue light emission can be attributed due to oxygen vacancies and indium-oxygen vacancy centers [30].

4. Conclusions

Cubic structured In_2O_3 thin films were formed on glass substrates by using an activated reactive evaporation method. The structure, optical and electrical properties of the films were highly influenced by the oxygen partial pressure. The films exhibited low electrical resistivity at lower oxygen partial pressure due to presence of un-oxidized indium and the electrical resistivity of the films increased with increase of oxygen partial pressure. At an optimum condition of oxygen partial pressure of 2×10^{-3} mbar, the films exhibited the electrical resistivity of $8.2 \times 10^{-4}\ \Omega$ cm, optical transmittance of 87% in the visible region and optical band gap of 3.62 eV. The figure of merit of the films increased from 1.14×10^{-3} to $6.4 \times 10^{-3}\ \Omega^{-1}$ with the increase of oxygen partial pressure. Two distinct peaks in the photoluminescence spectrum were observed at wavelengths of 415 and 440 nm. The films formed at the optimized oxygen partial pressure of 2×10^{-3} mbar are most suitable for the optoelectronic applications.

References

[1] E. Fortunato, D. Ginley, H. Hosono, D.C. Paine, Mater. Res. Soc. Bull. 32 (2007) 242.
[2] K. Hara, K. Sayama, H. Arakawa, Solar Energy Mater. Solar Cells 62 (2000) 441.
[3] N. Biyikli, T. Kartgoglu, O. Aytur, I. Kimukin, E. Ozbay, Appl. Phys. Lett. 79 (2001) 2838.
[4] S. Kaleemulla, A. Sivasankar Reddy, S. Uthanna, P. Sreedhara Reddy, Mater. Lett. 61 (2007) 4309.
[5] A. Subrahmanyam, U.K. Barik, J. Phys. Chem. Solids 66 (2005) 817.
[6] B. Radhakrishna, T.K. Subramanyam, B. Srinivasulu Naidu, S. Uthanna, Opt. Mater. 15 (2000) 217.
[7] A. Subrahmanyam, U.K. Barik, J. Phys. Chem. Solids 67 (2006) 1518.
[8] L.C. Chen, S.C. Liu, Solid State Electron. 50 (2006) 1355.
[9] M.H. Huang, Y. Wu, H. Feick, N. Tran, E. Weber, P. Yang, Adv. Mater. 13 (2001) 113.
[10] A. Bourlang, D.J. Payne, R.G. Egdell, J.S. Foord, P.P. Edwards, M.O. Jones, A. Schertel, P.J. Dobson, J.L. Hutchison, Appl. Phys. Lett. 92 (2008) 092117.
[11] P. Prathap, Y.P. Venkata Subbaiah, M. Devika, K.T. Ramakrishana Reddy, J. Mater. Chem. Phys. 100 (2006) 375.
[12] R.A. Sailer, A. Wanger, C. Schmit, N. Klaverkamp, D.L. Schulz, Surf. Coat. Technol. 203 (2008) 835.
[13] M.A. Flores, R. Castanedo, G. Torres, J. Marquez, O. Zelaya, Thin Solid Films 570 (2008) 681.
[14] A.V. Moholkar, C.M. Pawar, K.Y. Rajpure, V. Ganesan, C.H. Bhosale, J. Alloys. Compd. 464 (2008) 387.
[15] C.M. Ghimbeu, J. Schoonman, M. Lumbreras, Ceram. Int. 34 (2008) 95.
[16] W.H. Ho, C.F. Li, H.C. Liu, S.K. Yen, J. Power Sources 175 (2008) 897.
[17] J.L. van der Pauw, Philips Res. Rep. 13 (1958) 1.
[18] T.K. Subramanyam, B.S. Naidu, S. Uthanna, Appl. Surf. Sci. 169 (2001) 529.
[19] B.D. Cullity, Elements of X-ray Diffraction, 2nd ed., Addison Wesley, Reading, MA, 1978, p. 102.
[20] JCPDS [Code No: 6-0416].
[21] K.G. Gopchandran, B. Joseph, J.T. Abraham, P. Koshy, V.K. Vaidyan, Vacuum 48 (1997) 547.
[22] J. Tauc, Amorphous and Liquid Semiconductors, Plenum Press, New York, 1974.
[23] H.Y. Yeom, N. Popovich, E. Chason, D.C. Paine, Thin Solid Films 411 (2002) 17.
[24] T.K. Subramanyam, B. Radhakrishna, B.S. Naidu, P.J. Reddy, S. Uthanna, Vacuum 48 (1997) 565.
[25] G. Haacke, Ann. Rev. Mater. Sci. 7 (1977) 73.
[26] P. Nath, R.F. Bunshah, Thin Solid Films 69 (1980) 63.
[27] F.M. Amanullah, K.J. Pratap, V. Hari Babu, Thin Solid Films 254 (1995) 28.
[28] X. Li, W. Miao, Q. Zhang, L. Huang, Z. Zhang, Z. Hun, Semicond. Sci. Technol. 20 (2005) 823.
[29] S.Y. Sun, J.L. Huang, D.F. Lii, J. Vac. Sci. Technol. A 22 (2004) 1235.
[30] M.S. Lee, W.C. Choi, E. Kim, C.K. Kim, S.K. Min, Thin Solid Films 279 (1996) 1.
[31] P. Guha, S. Kar, S. Chaudhuri, Appl. Phys. Lett. 85 (2004) 3851.
[32] H.K. Kim, C.C. Li, G. Nykolak, P.C. Becker, J. Appl. Phys. 76 (1994) 8209.

Please cite this article in press as: S. Kaleemulla, et al., J. Alloys Compd. (2009), doi:10.1016/j.jallcom.2009.01.003